INSTITUTE OF PHYSICS PUBLISHING NANOTECHNOLOGY
Nanotechnology **18** (2007) 044009 (9pp) doi:10.1088/0957-4484/18/4/044009

Molecular mobility and transitions in complex organic systems studied by shear force microscopy

Tomoko Gray[1], Jason Killgore[1], Jingdong Luo[2], Alex K Y Jen[2] and René M Overney[1,3]

[1] Department of Chemical Engineering, University of Washington, Seattle, WA 98195-1750, USA
[2] Department of Material Science and Engineering, University of Washington, Seattle, WA 98195, USA

E-mail: roverney@u.washington.edu

Received 15 August 2006, in final form 2 November 2006
Published 12 December 2006
Online at stacks.iop.org/Nano/18/044009

Abstract
In this paper, we discuss novel nanoscale experimental approaches involving shear forces to investigate inter- and intramolecular mobilities, and their effect on mass and electronic transport, and material deformation properties. We review the non-scanning method of shear modulation force microscopy (SM-FM) used for glass transition analysis, and introduce heated tip atomic force microscopy (HT-AFM) for thermomechanical analysis of material interfaces. The dynamics and kinetics in organic thin films that are typically revealed by the activation energies related to molecular relaxations are determined with intrinsic friction analysis (IFA). Both SM-FM and IFA are applied to optimize the poling efficiency of organic non-linear optical materials involving chromophores, used for photonic devices. They also provide information about intramolecular relaxation properties. A shear force analysis involving HT-AFM was used to investigate the interfacial strength of silica nanoparticles and poly(trimethylsilylpropyne), which are known to form a reverse-selective membrane nanocomposite system.

(Some figures in this article are in colour only in the electronic version)

1. Introduction

Complex organic systems such as polymers or self-assembled molecular systems are particularly well suited for bottom-up, molecular design approaches. In solid state form, these systems are known to exhibit bulk deviating material and transport properties due to finite size limitations and interfacial constraints [16]. Practical examples are found in photonics [19], light emitting diode materials [18, 7], nanoelectromechanical systems (NEMS) [42], and organic and inorganic hybrid systems, such as nanocomposites [3, 38, 54]. A common way to gain fundamental insight into material and transport properties is to perform both a structural and a relaxation analysis. Typically, a relaxation analysis provides information about macroscopic stress–strain and stress–strain rate relationships, information about moduli and viscosity, and critical transitions such as the glass transition, T_g, or first- and second-order transitions, e.g., melting and order–disorder transitions, respectively. With more sophistication utilizing spectroscopy methods, such as neutron reflectivity (NR) and nuclear magnetic resonance (NMR), the molecular mobility can be inferred [49]. Today's challenge lies in obtaining convenient access to the molecular mobility of material arrangements that are interfacially constrained.

In this paper, we will discuss novel experimental approaches to investigate inter- and intramolecular mobilities, and their effect on mass and electronic transport, and material deformation properties. We will review the non-scanning method of shear modulation force microscopy (SM-FM) [4, 17] with which bulk T_g values have been accurately determined that correspond well to results

[3] Author to whom any correspondence should be addressed.

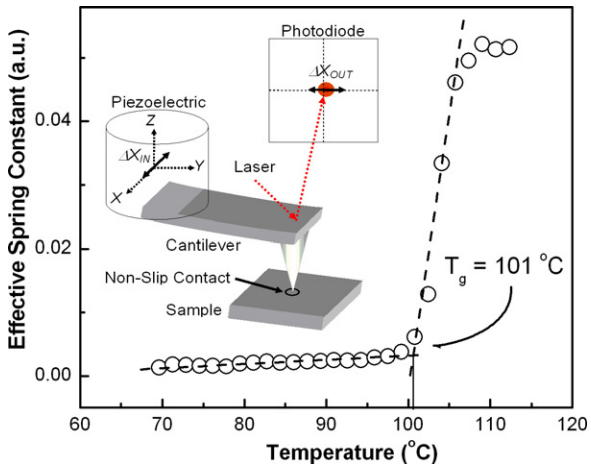

Figure 1. Working principle of shear modulation force microscopy (SM-FM).

from differential scanning calorimetry (DSC), and electron spin resonance (ESR) and agree with the theoretical molecular weight description of Fox-Flory [4]. SM-FM has also been successfully applied to determine bulk-deviating T_g of ultrathin polymer films with a thickness below ∼100 nm [9, 11, 15, 5, 51]. Regarding the investigation of the dynamics and kinetics in organic thin films that are typically revealed by the activation energies related to molecular relaxations, we will introduce an intrinsic friction analysis (IFA) [52]. In the first part of this paper, SM-FM and IFA, two complementary shear force methods, are applied to investigate the mobility of organic non-linear optical materials. The objective is to utilize side-chain mobilities to achieve increased acentric dipolar order, and thus, higher efficiencies of organic photonic devices. In the second part, we will address, with heated tip atomic force microscopy (HT-AFM), the interfacial interaction strength between dispersed nanoparticles and a polymer matrix. Thereby HT-AFM, generally applied towards obtaining thermomechanical properties [48, 13, 45], provides here a highly focused thermal shear disturbance, which leads to interfacial peeling of the inorganic nanocomposite component from its organic matrix at the appropriate temperature and load.

2. Instrumental and experimental

Since the introduction of scanning tunnelling microscopy (STM) by Binning and Rohrer in 1986 [2], the family of scanning probe microscopy (SPM) has grown to include many analysis tools. Among these surface tools, scanning force microscopy (SFM) is most widely used. When operated in contact mode, the SFMs cantilever probing tip forms a single asperity contact with the sample surface, and has been found to be an excellent tool for tribological (friction, adhesion, lubrication) studies [36]. Most of these experiments involve shear force (e.g., friction) measurements. The instrumental details of three extensions of shear force SFM methods, i.e., SM-FM, IFA and HT-AFM, are discussed below.

2.1. Shear modulation force microscopy (SM-FM)

SM-FM is a non-scanning method used to study structural transitions and thermally induced relaxations. Conceptually, SM-FM is a nanoscopic analogue to dynamic mechanical analysis (DMA). In essence, mechanical responses to external shear forces with varying temperature entail a material's viscoelastic properties, such as the modulus. The technique was originally introduced as a method to determine the contact area [36]. A lateral force, $\mathrm{d}F$, acting on a circular contact area, $A = \pi a^2$ (a is the contact radius) results in a lateral stress, $\mathrm{d}\tau$. In determining the contact area, the deformation responses of the test material, its strain $\mathrm{d}\gamma$, and strain rate $\mathrm{d}\gamma/\mathrm{d}t$ are important. Neglecting the rate dependence by assuming a fully elastic contact, the total strain is expressed as $\mathrm{d}u_x/a$, where $\mathrm{d}u_x$ is the lateral material deformation. The shear stress is then determined from Hook's law,

$$\mathrm{d}\tau = G\,\mathrm{d}\gamma \tag{1}$$

where G is the shear modulus of the material. For small lateral no-slip disturbances, the contact area can be assumed to be unaffected, and thus, the shear force is proportional to the product of modulus and strain. The effective spring constant, k_{eff}, is proportional to the product of the contact modulus and the contact radius. The total lateral displacement, $\mathrm{d}x$, combines both the sample deformation, $\mathrm{d}u$, and the spring deformation in the lateral direction. If the force is solely related to the sample deformation, the spring constant is referred to as the contact stiffness k_c. Contact stiffness and effective spring constant are related to each other via the cantilever lateral spring constant k_x as determined by equation (2).

$$k_{\mathrm{eff}} = \left(\frac{1}{k_c} + \frac{1}{k_x}\right)^{-1}. \tag{2}$$

The lateral spring constant can be determined quite accurately for any cantilever with a blind calibration method discussed elsewhere [58]. For a sphere–plane geometry, the contact stiffness is given as

$$k_c = 8G^* a \tag{3}$$

with the contact modulus $G^* = [(2 - \upsilon_{\mathrm{tip}})/G_{\mathrm{tip}} + [(2 - \upsilon_{\mathrm{sample}})/G_{\mathrm{sample}}]^{-1}$, where G_{tip} and G_{sample} are the tip and sample shear moduli, and υ_{tip} and $\upsilon_{\mathrm{sample}}$ are the tip and sample Poisson's ratios, respectively [36]. Since the tip modulus can be assumed not to change during the experiment, a change in k_c is a reflection of change in the sample modulus and the contact area.

The SM-FM method is briefly described as follows. A nanometre sharp SFM cantilever tip is brought into contact with the sample surface, figure 1 [40, 17]. While a constant load is applied, the probing tip is laterally modulated with a 'no-slip' nanometre amplitude, $\Delta X_{,\mathrm{IN}}$. The modulation response, ΔX_{OUT}, is analysed using a two-channel lock-in amplifier, comparing the response signal to the input signal. As previously mentioned, the modulation response, i.e., the effective stiffness, is a measure of the contact stiffness. Thermally activated transitions in the material, such as the glass transition, T_g, are determined from the 'kink' in the response curve, as documented in figure 1. SM-FM has proved to be particularly successful in determining glass transitions of ultrathin polymer films [4, 26] and the structural relaxations in nano-constrained or complex organic materials, such as for ionic copolymer electrolyte

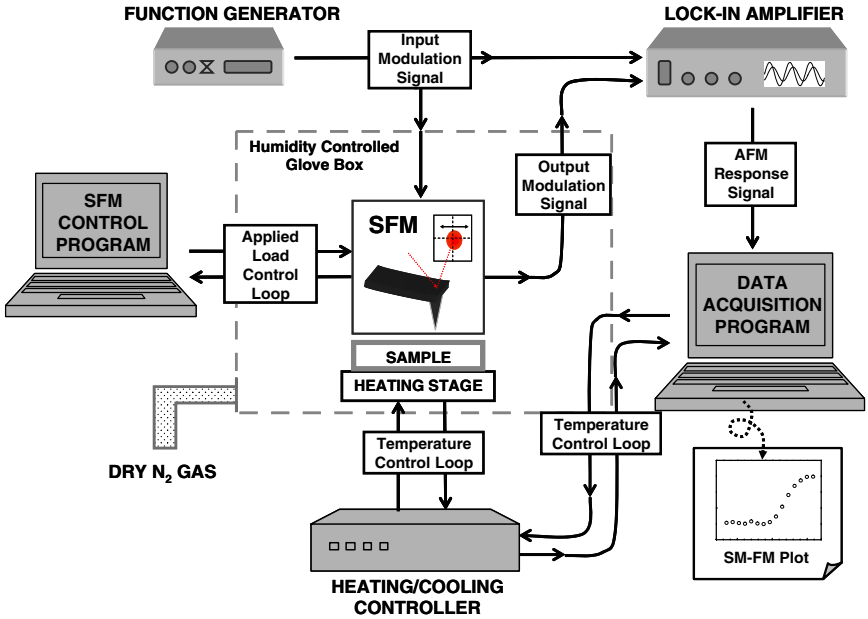

Figure 2. SM-FM experimental set-up. The equipment consists of: (1) SFM (Explorer, Veeco Instrument Inc.); (2) heating/cooling module (K-20 Programmable Temperature Controller, MMR Technologies, Inc); (3) lock-in amplifier (7280 DSP Lock-In Amplifier, Perkin Elmer Instrument); (4) function generator (DS345 30MHz Synthesized Function Generator, Stanford Research System); (5) SFM control program (Topometrix SPM Lab V4.0, Veeco Instrument Inc.); (6) glove box (custom made, Terra Universal); (7) data acquisition program (LabVIEW 5.0, National Instruments). Typical operational parameters are: (1) relative humidity ∼5%; (2) input modulation 0.1 V (1–10 nm); (3) applied normal load 10–100 nN; (4) heating rate 0.1–0.5 °C min^{-1}.

membranes (Nafion®) [58], perfluoropolyether lubricants (Fomblin Zdol®) [43], crosslinked hexafluoropropylene for bio-compatibility [26], *N*-isopropylacrylamide (NIPAM) gels for drug delivery [40], and dendronized non-linear optical side-chain chromophore polymers for photonic applications [19], which will be further discussed below. The entire experimental set-up of SM-FM is provided in figure 2.

2.2. *Intrinsic friction analysis (IFA)*

IFA is based on the well-established lateral force microscopy [41]. While SM-FM probes thermally activated structural transitions, IFA provides molecular descriptions of relaxation processes that are associated with structural transitions. This is interesting from the perspective that frictional sliding with nano-scaled probes provides the means to transfer kinetic energy very specifically to internal modes on a molecular or even submolecular level, as shown recently by activating side chain rotations in glassy polystyrene [52], and backbone translational motions in polymer melts [50].

The IFA is briefly described as follows: based on the lateral force microscopy, the friction force is determined from the hysteresis in the torsional cantilever deflection between forward and reverse scans. In order to deduce the apparent activation energy of the segmental motion, friction forces that are obtained at varying scanning velocity and temperature are treated based on the theory of time–temperature equivalence [57, 14]. Friction–velocity isotherms, $F_F(v)$, are "segments of a single 'master curve"' [20] which describe the relaxation landscape of a material similar to dielectric permittivity ε'' and loss modulus G'' [22, 14]. Due to

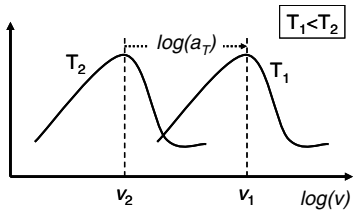

Figure 3. Schematic of the time–temperature equivalence and superposition principle applied to IFA.

the limitation in the experimental velocity and the temperature range, the shape of the isotherms are observed as log-linear curves, or as bell-shaped curves with characteristic peaks at critical velocities where the Deborah number is one, i.e. the experimental times τ_e match the characteristic relaxation times τ_m. This is schematically shown in figure 3. The friction–velocity isotherms at temperature T_1 and T_2 where $T_1 < T_2$ display the characteristic peaks at the critical velocities of v_1 and v_2. In order to form a master curve, an isotherm curve at a reference temperature (e.g. T_1) is arbitrarily chosen. The other isotherm curves are then superimposed to the reference isotherm by shifting them with horizontal distances $\ln(a_T)$, where a_T is the thermal shift factor. When the isotherms show a characteristic peak, the peak will be a convenient reference point for forming a reliable master curve. It should be noted that the height of the peak $F_F(v_{max})$ varies with the strength of the corresponding relaxation process, therefore normalization might be necessary. This treatment is commonly done with dielectric spectroscopy analyses and is also applicable to other relaxation analyses, as shown by Ferry [14].

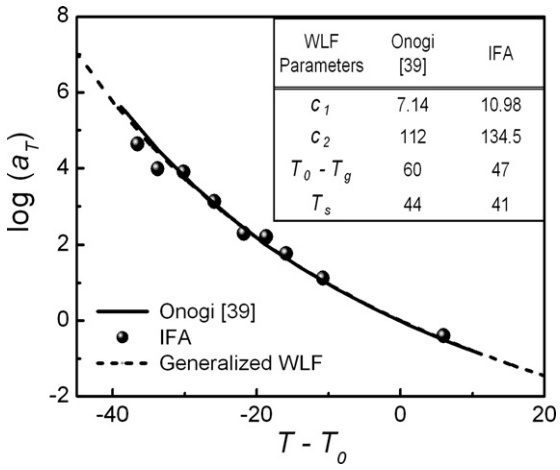

Figure 4. The shift factor plotted against reduced temperature for rubbery polystyrene and Ferry's generalized WLF curve. Inset: WLF parameters from literature [39] and IFA.

Once the thermal shift factors, a_T, for each temperature are obtained, the apparent activation energy can be deduced from a plot of $\ln(a_T)$ as a function of inverse temperature, $1/T$. The linear dependence of $\ln(a_T)$ on $1/T$, known as the Arrhenius form of relaxation, describes a purely kinetic process (i.e., entropic process). The activation energy is determined from [57],

$$\Delta E_a = -R\left[\frac{\partial \ln(a_T)}{\partial(1/T)}\right]_P \tag{4}$$

where ΔE_a is the activation energy and R is the ideal gas constant. The relationship becomes non-linear (i.e., non-Arrhenius) for processes that also involve changes in the enthalpy, as in the case of the α-relaxation. The activation energy then follows a temperature relation expressed by the Williams–Landel–Ferry (WLF) equation [14]:

$$\Delta E_a = 2.303 R c_1 c_2 \frac{T^2}{(c_2 + T - T_0)^2} \tag{5}$$

where R is the ideal gas constant, and c_1 and c_2 are material specific constants that are obtained by plotting $-(T - T_0)/\log(a_T)$ against $(T - T_0)$.

SM-FM and IFA, used to determine T_g and the relaxation dynamics, respectively, complement each other, and therefore are most valuable when combined. These two techniques were previously applied on polystyrene thin films (>200 nm thick, 96.5 K M_w). In the glassy state, the available relaxation mode of the γ relaxation (7 kcal mol^{-1}), which shows Arrhenius behaviour, was determined by equation (4) [52]. However, in the rubbery state the WLF expression (equation (5)) was applied. The determined WLF parameters $c_1 = 10.98$ and $c_2 = 134.5$ were comparable to the values reported by Onogi *et al* [39], figure 4. The values also show fairly good agreement with Ferry's generalized parameters $c_1 = 8.86$ and $c_2 = 101.6$. The appropriate reference temperature $T_s = 41\,^\circ$C was determined by fitting to Ferry's generalized curve. The value of 41 °C from the IFA method agrees well with the 44 °C of Onogi *et al* [39] and the 45 °C found by Williams *et al* [59]. The corresponding activation energy for the α-relaxation was determined to vary from 115 kcal mol^{-1} at 104 °C to 65.8 kcal mol^{-1} at 147 °C.

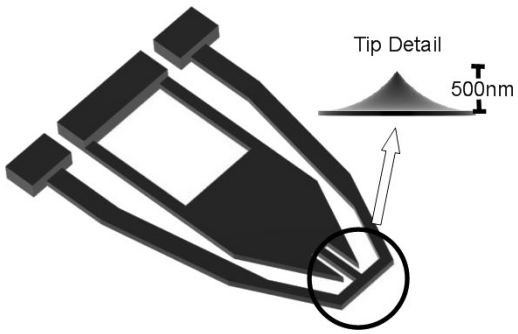

Figure 5. Schematic of IBM HT-AFM cantilever tip typical of the design used in this study.

2.3. Heated tip atomic force microscopy (HT-AFM)

HT-AFM uses variably doped resistive cantilever materials to integrate heating directly into the cantilever probe. The technique was originally commercialized by TA-Instruments as the Micro-TA 2990; however, as the name suggests, the resolution of these units was orders of magnitude less than their non-heated AFM counterparts [45, 46, 21]. This resolution limitation was later addressed by IBM during the development of their Millipede high-density data storage project [12, 13, 55]. Unlike the Micro-TA probes that used a wire as both heater and probe, the Millipede design uses a 500 nm tip located on a small heater stage (figure 5) [12, 48, 56]. Although providing less efficient heat transfer, the set-up allows for a more conventional, i.e., nanoscopically sharp, tip design.

Using a stationary probe position and a ramped voltage increase, it is possible to perform local nano-thermomechanical analysis on a variety of polymer systems. In addition to thermomechanical analysis, the substrate can be scanned at various tip temperatures. With the heated scanning approach, it is possible to physically manipulate the sample. By quantifying the forces required for such manipulation, processes such as interfacial debonding can be investigated locally, as discussed below.

Basic temperature calibration is performed by assuming that the heater temperature is proportional to the input power. The input power is determined by monitoring voltage and current at the lever. The maximum temperature of the tip is 550 °C and maximum power is defined by a sharp hook in the I–V curve. The equilibrium temperature of the tip is then given by:

$$T_{eq} = T_{rm} + \frac{(T_{max} - T_{rm})}{P_{max}} P \tag{6}$$

where T_{eq}, T_{rm}, P_{max} and P are the equilibrium temperature of the heater, surrounding temperature (room temperature), maximum power, and instantaneous power, respectively.

Compared to substrate heating methods, e.g., SM-FM, HT-AFM offers some distinct advantages. Foremost is the ability to heat locally to higher temperatures. With substrate heating, conductive or convective heating significantly impact temperature variations away from the sample causing undesired thermal expansions (drifts) within the AFM. Furthermore, if global substrate heating is used, critical AFM system components can overheat. For instance,

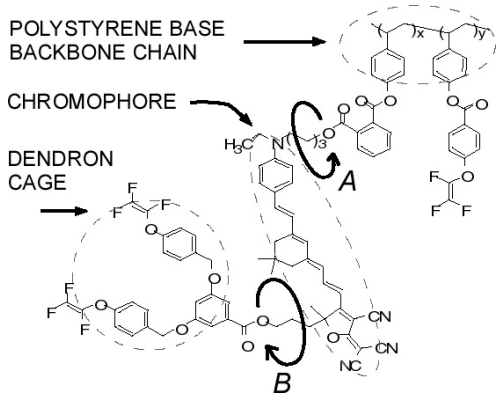

Figure 6. Chemical structure of PS-CLD1 and the local segmental mobilities of PS-CLD1at *A* and *B*.

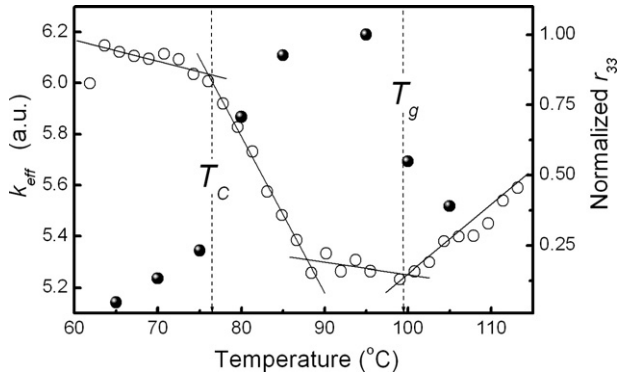

Figure 7. SM-FM measurement (○) of PS-CLD1 identifies two transitions, T_c at 79 °C and T_g at 99 °C, and EO activity coefficient r_{33} (●) as a function of the poling temperature [19].

piezo ceramics start to depole above 80 °C. Other advantages of HT-AFM over global sample heating include the ability to operate at very high heating rates due to the low thermal mass, and the ability to perform multiple measurements on specimens that are highly sensitive to thermal history.

2.4. Sample preparation and specifics about instrumentation

PS-CLD1 [27], a dendronized non-linear optical (NLO) polymer, thin films were spin-cast onto indium tin oxide (ITO) coated glass substrates from a 0.2 μm filtered 13% PS-CLD1 solution dissolved in cyclopentanone. The resulting films, with thickness of the order of 1 μm, were annealed at 85 °C in a vacuum oven for over 12 h.

Poly(trimethylsilylpropyne), PTMSP, with >95% purity was obtained from Gelest, Inc. 200 nm diameter silica particles were prepared by mixing 200 ml anhydrous ethanol, 6 ml tetraethyl orthosilicate and 12 ml of 30 wt% ammonia in water in a glass beaker. The solution was stirred for 12 h, then dried and redispersed in toluene. Trace amounts of the silica–toluene dispersion were mixed with pure toluene to produce a dilute silica–toluene dispersion. PTMSP was added to the silica–toluene dispersion to make a 3 wt% solution. The solution was spin cast onto a glass substrate, producing film thickness of ∼1 μm.

IFA, HT-AFM and SM-FM experiments were conducted under nitrogen with relative humidity below ∼10% to avoid capillary necks. IFA and SM-FM used bar shaped silicon cantilevers (Nanosensors, normal spring constants between 0.1 and 0.15 N m^{-1}, and lateral spring constants of 80–100 N m^{-1}). The normal spring constant, k_N, for bar shaped and bare silicon cantilevers is rather well determined (error <10%) with

$$k_N = \frac{E w t^3}{4l^2} \tag{7a}$$

$$t = 6.190\,415\sqrt{\frac{\rho}{E}} f_1 l^2 \tag{7b}$$

where l, w, t are the length, width, thickness of the cantilever, respectively, E is the Young's modulus and ρ is the density of silicon [37, 36]. The first resonance frequency in the normal direction, f_1, is measured. The lateral spring constant was determined with the above mentioned blind calibration method [6, 58].

SM-FM and IFA measurements were obtained within a normal load range of 5–100 nN, modulation amplitudes on the order of 5–10 nm, and a frequency range of 4–5 kHz. The sample temperature was increased stepwise by 0.5–2.0 °C at a rate of 2–5 °C min^{-1}. The system was calibrated on bulk polystyrene (PS) films with a thickness above 200 nm. IFA measurements were performed at scan velocities ranging from 200 nm s^{-1} to 8 μm s^{-1}, and at temperatures ranging from 49 to 111 °C. A total normal force of 90 nN was chosen arbitrarily for all temperatures.

Thermomechanical HT-AFM measurements were conducted at a heating rate of 60 °C min^{-1} while monitoring the Z piezo voltage with the feedback loop engaged. Heated tip scans were performed at a 1 μm s^{-1} scan speed. Maximum probe–particle impact deflection was determined from the lateral force microscopy image. Deflection was converted to impact force by calibrating the probe's lateral spring constant on a silicon wafer ⟨1, 1, 1⟩ of known friction coefficient (see blind calibration method [6, 58]).

3. Results and discussion

3.1. Low temperature relaxation of non-linear optical side-chain polymers

Organic second-order non-linear optical (NLO) materials have shown great potential in broadband communication, high-density data storage and ultrahigh speed electro-optic (EO) switches [29, 8]. While recent advances in the design of chromophores enhanced the non-linearity by more than two orders of magnitude [8], translation of the high molecular non-linearity into large macroscopic EO activities is a major challenge [47, 24]. In general, EO activity is induced by poling within an electric field normal to the NLO surface, which causes the chromophore to order acentrically [30]. The poling process commonly utilizes the high molecular mobility above the glass transition temperature T_g of the material [60, 28, 53]. However, high mobility also promotes undesired aggregation of the highly dipolar chromophores. Annihilation of non-linearity is a result of such aggregation.

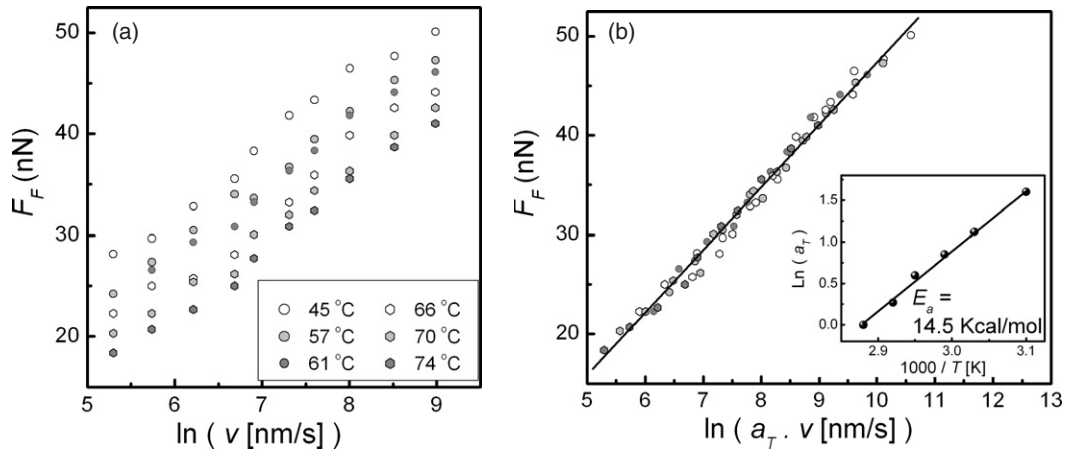

Figure 8. IFA of PS-CLD1for $T < T_c$. The friction–velocity isotherms (a) were shifted by the thermal shift factor $\ln(a_T)$ to form the superimposed 'master curve' (b). Inset: the Arrhenius plot of the thermal shift factor as a function of the inverse of temperature yields an activation energy E_a of 14.5 kcal mol^{-1}.

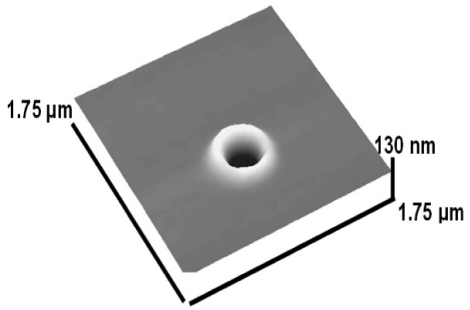

Figure 9. Thermomechanical analysis indentation on PTMSP showing a 130 nm deep hole with a 35 nm rim. Rim to rim diameter is ∼500 nm.

The specifically designed structure of our dendronized NLO side-chain polymer, PS-CLD1 [27] (figure 6), addresses this particular problem. Highly dipolar chromophores are protected from aggregation by a bulky dendritic moiety, which is attached to the main polystyrene-based backbone chain for better control of the molecular mobility. A drawback of this structure is the embodiment of long chains and bulky moieties which reduce the efficiency of chromophore alignment. Thus, a detailed assessment of the molecular mobility is essential for determining an appropriate temperature window for optimized poling.

Our first approach was to search with SM-FM for critical transitions below T_g that would allow for low temperature poling. As presented in figure 7, we found a transition about 20 °C below the glass transition temperature (99 ± 1 °C) at $T_c = 77 \pm 1$ °C [19]. This transition was not obtainable with DSC. Guided by SM-FM, we performed a series of poling experiments from 60 to 120 °C, in order to investigate poling in relation to T_c and T_g. As shown in figure 7, below T_c, the EO coefficient, r_{33}, was low and increases linearly with temperature. However, r_{33} nearly quadrupled above T_c, thus indicating that significantly higher acentric order of the chromophores is achieved. Above T_g, the EO efficiency drops again because of undesired aggregation.

The molecular description of the low temperature relaxation process of PS-CLD1 is provided by IFA. Analogous to prior experiments described above [52, 50], we obtained activation energy from the friction values obtained at varying scanning velocity and temperature. In the temperature range below T_c, the friction–velocity isotherms formed a series of parallel log-linear curves (figure 8(a)). According to time–temperature equivalence [57], the isotherms were shifted horizontally by the thermal shift factor $\ln(a_T)$ to form a 'master curve' at a reference temperature, T_0, of 74 °C, as shown in figure 8(b). Knowing that the system is in a glassy state in this temperature range, the Arrhenius relation (equation (4)) was appropriately used. An activation energy of 14.5 kcal mol^{-1} was determined (inset of figure 8(b)). Similarly, we also obtained the activation energy in the temperature range between T_c and T_g. Note that the system is still in the glassy state in this temperature range, thus the Arrhenius relation was applied and the energy value was determined to be 24.2 kcal mol^{-1}.

According to Heijboer's treatment [23], and a comparable study of activation energies of dendrimers by Kwak and co-workers [25], the relaxation mode below T_c is considered to be a relaxation of the Fréchet-type, a dendritic moiety, indicated as '*B*' in figure 6. Similarly, the relaxation mode in between T_c and T_g originates from the mobility of flexible linkage at the base of the dendrimer-grafted-chromophore containing side chain as indicated by '*A*' in figure 6.

3.2. Thermally assisted shearing on nanocomposite membranes

Unlike traditional composite materials whose properties are influenced largely by the constituent components, nanocomposites exhibit such large specific surface areas that interfacial properties can significantly affect bulk behaviour. PTMSP, poly(trimethylsilylpropyne), has garnered attention since its discovery due to its very high permeability, high T_g and exhibited reverse selectivity [31, 32]. However, it was the discovery that the permeability and reverse selectivity could be significantly enhanced by the addition of silica nanoparticles that has generated most recent interest in the material [33, 34, 10, 44, 1]. This enhancement was particularly significant because it contradicted the Maxwell equation,

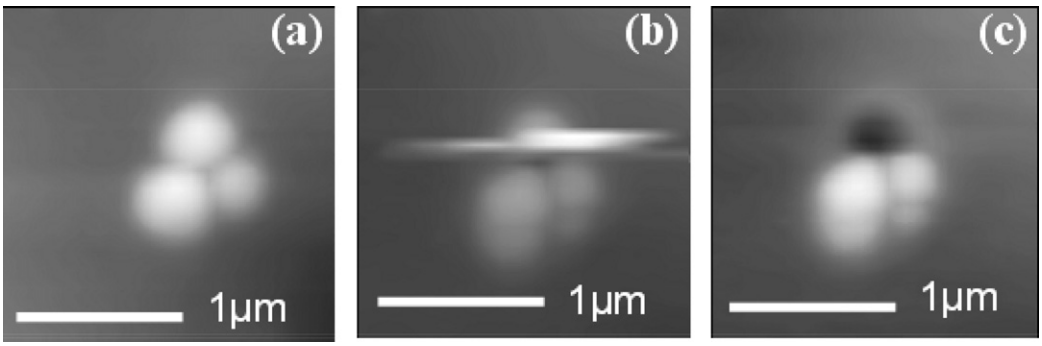

Figure 10. Series of scanning heated tip images taken at tip temperatures at 220 °C (a), 290 °C (b) and 300 °C (c). The streaking in image (b) shows the debonding event and subsequent dragging of the particle.

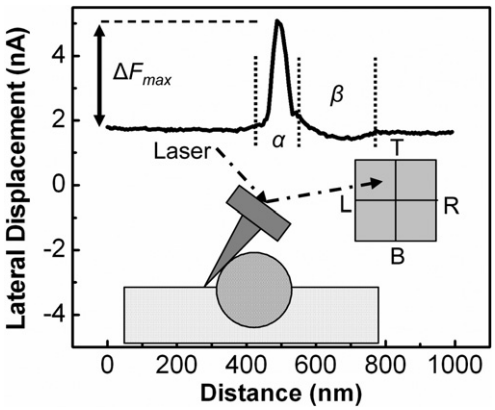

Figure 11. Characteristic forward friction scan across stable silica particle when scanned with heated tip. α corresponds to the particle impact, whereas β identifies the friction associated with the SiO_2 particle.

which predicts a reduction in permeability with the addition of an impermeable phase. Further studies on filler size and surface chemistry suggested that the addition of silica resulted in an increased fractional free volume in the polymer [35]. While the importance of the nanoscale PTMSP–silica interface has been acknowledged, most of the data currently published is based on macroscopic rather than microscopic measurements, and thus, little is known about the local nanoscale properties of the material.

Nano-thermomechanical analysis by HT-AFM on PTMSP membranes revealed a transition, which is consistent with the indentation behaviour typically observed during the glass transition, at a heater temperature of $T^* = 190\,^{\circ}\mathrm{C}$ using a $60\,^{\circ}\mathrm{C\,min^{-1}}$ heating rate. Figure 9 shows the thermomechanical analysis hole pattern from the temperature scan on PTMSP. The tip radius is approximately 10 nm and the local heating area prior to tip penetration is less than 100 nm. Due to the relatively fast heating rate, tip penetration occurs quickly after T^*. The lack of thermal drift in the technique is evident by the symmetry of the hole.

When operating the heated tip in lateral scanning mode, the tip is constantly moving, and the sample never reaches thermal equilibrium with the tip, and thus is not heated to the same extent as for a stationary tip. As a result, it is possible to scan above T^* without initiating severe plastic surface deformation. The actual temperature at the surface depends on contact resistance, tip temperature, and scan speed. Figure 10 shows a series of heated tip scans on a PTMSP composite taken at tip temperatures above T^*. The HT-AFM is operated over a region with exposed silica particles, with increasing temperature increments of 10 °C for each new scan. When a critical temperature is reached (290 °C for the series in figure 10), the forces acting on the particle, coupled with thermally induced interfacial instabilities, are sufficient to debond the particle from the matrix. The lack of a noteworthy matrix deformation around the particle suggests that the debonding occurred below T^* without plastic alteration of the bulk polymer matrix.

The lateral forces associated with debonding were determined by investigating the lateral force microscopy signal. Figure 11 shows a characteristic lateral force scan. The large peak α, identified by the lateral force difference ΔF_{max} from the friction baseline of PTMSP, is associated with the torsional deflection of the cantilever as the tip contacts the particle. Eventually, the tip slides past the contact point and a slight decrease in friction relative to the matrix is observed (see β in figure 11). This decrease is a result of the different coefficients of friction between the particle and the matrix. The dependence of the lateral force on temperature, for another thermally debonded particle, was determined by finding the local L-R signal maximum at the polymer–particle interface from the series of temperature scans. As shown in figure 12, increasing temperature above ∼160 °C leads to increasing ΔF_{max} values. The impact force is relatively constant below 160 °C. This region below 160 °C, identified as α_1 in figure 12, corresponds to the baseline originating from the nanoparticle induced topographic cross-talk. The higher force region, identified as α_2 in figure 12, corresponds to the progressive interfacial failure force imparted on the particle with increased temperature. The maximum observed force at 10 °C below the debonding temperature was 220 nN. These initial debonding experiments illustrate the potential of HT-AFM towards adhesive bond strength measurements between embedded inorganic nanoparticles and their organic matrix.

4. Summary

Novel shear force microscopy techniques were applied to study two advanced functional systems, non-linear optical materials and nanocomposite polymer membranes. The instrumental

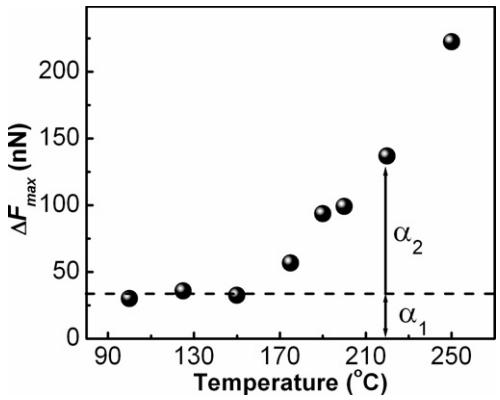

Figure 12. Maximum lateral force subjected to particle as a function of temperature. ΔF_{max} is measured from the baseline PTMSP friction.

demands for working with homogeneous and heterogeneous materials have led to different analytical techniques. SM-FM and IFA have been applied to identify relaxation temperatures, as well as the respective intramolecular motions available within different temperature regimes, to optimize the EO and guide the development of new NLO materials. In the case of the PTMSP reverse-selective membrane, surface heterogeneity and high transition temperatures necessitated the use of a heated AFM tip rather than a heated substrate. HT-AFM was used to identify the local transition temperature of the composite film, while also acting as a manipulating tool for investigating the particle-matrix debonding strength, on which improved nanocomposite membranes rely.

Acknowledgments

The authors would like to thank the IGERT graduate fellowship through the Centre of Nanotechnology at the University of Washington, and the National Science Foundation (NSF-NIRT and the NSF-STC Program under Agreement No. DMR-0120967). The authors would also like to thank the Petroleum Research Fund administered by the American Chemical Society, the Boeing Company for their graduate student support, as well as IBM, Zurich and Anasys Inc. for their heated tip AFM equipment support and expertise.

References

[1] Andrady A L, Merkel T C and Toy L G 2004 Effect of particle size on gas permeability of filled superglassy polymers *Macromolecules* **37** 4329–31

[2] Binnig G, Quate C F and Gerber G C 1986 Atomic force microscope *Phys. Rev. Lett.* **56** 930–3

[3] Breuer O and Sundararaj U 2004 Big returns from small fibers: a review of polymer/carbon nanotube composites *Polym. Compos.* **25** 630–45

[4] Buenviaje C, Dinelli F and Overney R M 2000 Glass transition measurments of ultrathin polymer films *ACS Symp. Series 'Interfacital Properties on the Submicron Scale'* ed J Frommer and R M Overney (New Orleans: Oxford University Press) pp 76–92

[5] Buenviaje C, Ge S, Rafailovich M, Sokolov J, Drake J M and Overney R M 1999 Confined flow in polymer films at interfaces *Langmuir* **15** 6446–50

[6] Buenviaje C K, Ge S R, Rafailovich M H and Overney R M 1998 Atomic force microscopy calibration methods for lateral force, elasticity, and viscosity *Mater. Res. Soc. Symp. Proc.* **522** 187–92

[7] Campoy-Quiles M, Sims M, Etchegoin P G and Bradley D D C 2006 Thickness-dependent thermal transition temperatures in thin conjugated polymer films *Macromolecules* **39** 7673–80

[8] Dalton L R *et al* 1999 From molecules to opto-chips: organic electro-optic materials *J. Mater. Chem.* **9** 1905–20

[9] de Gennes P-G 2000 Glass transitions of freely suspended polymer films *C. R. Acad. Sci.* **4** 1–8

[10] De Sitter K, Winberg P, D'Haen J, Dotremont C, Leysen R, Martens J A, Mullens S, Maurer F H J and Vankelecom I F J 2006 Silica filled poly(1-trimethylsilyl-1-propyne) nanocomposite membranes: relation between the transport of gases and structural characteristics *J. Membr. Sci.* **278** 83–91

[11] Dinelli F, Buenviaje C and Overney R M 2000 Glass transitions of thin polymeric films: speed and load dependence in lateral force microscopy *J. Chem. Phys.* **113** 2043–8

[12] Durig U *et al* 2000 'Millipede'—an AFM data storage system at the frontier of nanotribology *Tribol. Lett.* **9** 25–32

[13] Eleftheriou E *et al* 2003 Millipede—A MEMS-based scanning-probe data-storage system *IEEE Trans. Magn.* **39** 938–45

[14] Ferry J D 1980 *Viscoelastic Properties of Polymers* (New York: Wiley)

[15] Forrest J A and Mattsson J 2000 Reductions of the glass transition temperature in thin polymer films: probing the length scale of cooperative dynamics *Phys. Rev.* E **61** R53–61

[16] Frommer J and Overney R M (ed) 2001 *Interfacial Properties on the Submicron Scale* vol 781 (Oxford: Oxford University Press)

[17] Ge S, Pu Y, Zhang W, Rafailovich M, Sokolov J, Buenviaje C, Buckmaster R and Overney R M 2000 Shear modulation force microscopy study of near surface glass transition temperatures *Phys. Rev. Lett.* **85** 2340–3

[18] Gray T, Buenviaje C, Overney R M, Jenekhe S A, Zheng L and Jen A K Y 2003 Nanorheological approach for characterization of electroluminescent polymer thin films *Appl. Phys. Lett.* **83** 2563–5

[19] Gray T, Overney R M, Haller M, Luo J and Jen A K Y 2005 Low temperature relaxations and effects on poling efficiencies of dendronized non-linear optical side-chain polymers *Appl. Phys. Lett.* **86** 211908

[20] Grosch K A 1963 The relation between the friction and visco-elastic properties of rubber *Proc. R. Soc.* A **274** 21–39

[21] Hammiche A, Reading M, Pollock H M, Song M and Hourston D J 1996 Localized thermal analysis using a miniaturized resistive probe *Rev. Sci. Instrum.* **67** 4268–74

[22] Hedvig P 1977 *Dielectric Spectroscopy of Polymers* (New York: Wiley)

[23] Heijboer J 1978 *Molecular Basis of Transitions and Relaxations* ed D J Meier (London: Gordon and Breach Science Publishers) pp 75–102

[24] Kajzar F, Lee K-S and Jen A K-Y 2003 Polymeric materials and their orientation techniques for second-order nonlinear optics *Adv. Polym. Sci.* **161** (Polymers for Photonics Applications II) 1–85

[25] Kwak S Y, Choi J and Song H J 2005 Viscoelastic relaxation and molecular mobility of hyperbranched poly(ε-caprolactone)s in their melt state *Chem. Mater.* **17** 1148–56

[26] Luginbuhl R, Overney R M and Ratner B D 2001 Nanobiotribology at the confined biomaterial interface *ACS Symp.: Interfacial Properties on the Submicrometer Scale* **781** 178–96

[27] Luo J, Liu S, Haller M, Liu L, Ma H and Jen A K-Y 2002 Design, synthesis, and properties of highly efficient side-chain dendronized nonlinear optical polymers for electro-optics *Adv. Mater.* **14** 1763–8
[28] Ma H, Jen A K-Y and Dalton L R 2002 Polymer-based optical waveguides: Materials, processing and devices *Adv. Mater.* **14** 1339–65
[29] Ma H, Liu S, Luo J, Suresh S, Liu L, Kang S H, Haller M, Sassa T, Dalton L R and Jen A K-Y 2002 Highly efficient and thermally stable electro-optical dendrimers for photonics *Adv. Funct. Mater.* **12** 565–74
[30] Marder S R and Perry J W 1994 Nonlinear optical polymers: discovery to market in 10 years? *Science* **263** 1706–7
[31] Masuda T, Isobe E, Higashimura T and Takada K 1983 Poly[1-(trimethylsilyl)-1-propyne]: a new high polymer synthesized with transition-metal catalysts and characterized by extremely high gas permeability *J. Am. Chem. Soc.* **105** 7473–4
[32] Masuda T, Tang B Z, Tanaka A and Higashimura T 1986 Mechanical properties of substituted polyacetylenes *Macromolecules* **19** 1459–64
[33] Merkel T C, Freeman B D, Spontak R J, He Z, Pinnau I, Meakin P and Hill A J 2002 Ultrapermeable, reverse-selective nanocomposite membranes *Science* **296** 519–22
[34] Merkel T C, He Z, Pinnau I, Freeman B D, Meakin P and Hill A J 2003 Effect of nanoparticles on gas sorption and transport in poly(1-trimethylsilyl-1-propyne) *Macromolecules* **36** 6844–55
[35] Merkel T C, Toy L G, Andrady A L, Gracz H and Stejskal E O 2003 Investigation of enhanced free volume in nanosilica-filled poly(1-trimethylsilyl-1-propyne) by 129Xe NMR spectroscopy *Macromolecules* **36** 353–8
[36] Meyer E, Overney R, Dransfeld K and Gyalog T 1998 *Nanoscience: Friction and Rheology on the Nanometer Scale* (Singapore: World Scientific)
[37] Nonnenmacher M, Greschner J and Wolter O 1991 Scanning force microscopy with micromachined silicon sensors *J. Vac. Sci. Technol.* B **9** 1358
[38] Okada A, Kawasumi M, Kurauchi T and Kamigaito O 1987 Synthesis and characterization of a nylon 6-clay hybrid *Polymer Preprints (American Chemical Society, Division of Polymer Chemistry)* **28** 447–8
[39] Onogi S, Masuda T and Kitagawa K 1970 Rheological properties of anionic polystyrenes. I. Dynaic viscoelasticity of narrow-distribution polystyrenes *Macromolecules* **3** 109–16
[40] Overney R M, Buenviaje C, Luginbuehl R and Dinelli F 2000 Glass and structural transitions measured at polymer surfaces on the nanoscale *J. Thermal Anal. Cal.* **59** 205–25
[41] Overney R M, Guo L, Totsuka H, Rafailovich M, Sokolov J and Schwarz S A 1997 Interfacially confined polymeric systems studied by atomic force microscopy *Dynamics in Small Confining Systems IV* ed J M Drake *et al* (Pittsburg, PA: Material Research Society) pp 133–44
[42] Overney R M and Sills S 2005 *Fundamentals of Nanoindentation and Nanotribology III* ed K Wahl *et al* (Warrendale, PA: Material Research Society) p R.5.1.-13
[43] Overney R M, Tyndall G and Frommer J 2004 *Handbook of Nanotechnolgy* ed B Bhushan (Heidelberg: Springer)
[44] Prabhakar R S, Merkel T C, Freeman B D, Imizu T and Higuchi A 2005 Sorption and transport properties of propane and perfluoropropane in poly(dimethylsiloxane) and poly(1-trimethylsilyl-1-propyne) *Macromolecules* **38** 1899–910
[45] Reading M, Hourston D J, Song M, Pollock H M and Hammiche A 1998 Thermal analysis for the 21st century *Am. Lab. (Shelton, Connecticut)* **30** 13–7
[46] Reading M, Price D M, Pollock H M, Hammiche A and Murray A 1999 Recent progress in microthermal analysis *Am. Lab. (Shelton, Connecticut)* **31** 13–6
[47] Robinson B H and Dalton L R 2000 Monte Carlo statistical mechanical simulations of the competition of intermolecular electrostatic and poling-field interactions in defining macroscopic electro-optic activity for orgainc chromophore/polymer materials *J. Phys. Chem.* A **104** 4785–95
[48] Sills S, Overney R M, Gotsman B and Frommer J 2005 Strain shielding and confined plasticity in thin polymer films: impacts on thermomechanical data storage *Tribol. Lett.* **19** 9–15
[49] Sillescu H 1999 Heterogeneity at the glass transition: a review *J. Non-Cryst. Solids* **243** 81–108
[50] Sills S, Gray T and Overney G 2005 Molecular dissipation phenomena of nanoscopic friction in the heterogeneous relaxation regime of a glass former *Chem. Phys. Lett.* **123** 134902
[51] Sills S, Overney R, Wilson C, Lee V, Miller R and Frommer J 2004 Interfacial glass transition profiles in ultrathin, spin cast polymer films *J. Chem. Phys.* **120** 5334–8
[52] Sills S and Overney R M 2003 Creeping friction dynamics and molecular dissipation mechanisms in glassy polymers *Phys. Rev. Lett.* **91** 095501
[53] Teraoka I, Jungbauer D, Reck B, Yoon D Y, Twieg R and Willson C G 1991 Stability of nonlinear optical characteristics and dielectric relaxations of poled amorphous polymers with main-chain chromophores *J. Appl. Phys.* **69** 2568–76
[54] Vassileva E and Friedrich K 2003 Epoxy/alumina nanoparticle composites. I. Dynamic mechanical behavior *J. Appl. Polym. Sci.* **89** 3774–85
[55] Vettiger P *et al* 2001 *Transducers '01. Eurosensors XV. 11th Int. Conf. on Solid State Sensors and Actuators* ed E Obermeier (Berlin: Springer) pp 1054–7
[56] Vettiger P, Despont M, Duerig U, Lantz M A, Rothuizen H E and Binnig G K 2003 *AFM-based Mass Storage—the Millipede Concept* pp 687–701
[57] Ward I M 1971 *Mechanical Properties of Solid Polymers* (London: Wiley–Interscience)
[58] Wei J H, He M and Overney R M 2006 Direct measurement of nanofluxes and structural relaxations of perfluorinated ionomer membranes by scanning probe microscopy *J. Membr. Sci.* **279** 608–14
[59] Williams M L, Landel R F and Ferry J D 1955 The temperature dependence of relaxation mechanisms in amorphous polymers and other glass-forming liquids *J. Am. Ceram. Soc.* **77** 3701–7
[60] Winkelhahn H-J, Servay T K and Neher D 1996 A novel concept for modeling the time–temperature dependence of polar order relaxation in nonlinear optical active polymers *Phys. Chem.* **100** 123–33